Resolution limits for optical transillumination of abnormalities deeply embedded in tissues

A. H. Gandjbakhche,[a] R. Nossal,[a] and R. F. Bonner[b]
National Institutes of Health, Bethesda, Maryland 20892

(Received 2 June 1993; accepted for publication 7 October 1993)

Random walk theory is used to calculate the line spread function (LSF) of photons as they cross the midplane of a slab of finite thickness. The relationship between the LSF and the photon transit time in transillumination time-resolved experiments is investigated. It is found that the LSF is approximately Gaussian distributed, with a standard deviation, σ, which can be used as a criterion of the spatial resolution of the imaging system. Results are substantiated by comparison with actual data in the literature. Any given resolution can be improved by reducing the excess transit time Δt, but heterogeneity of the scattering medium and low levels of detected light enormously complicate the achievement of subcentimeter spatial resolution. The latter point is discussed by using optical parameters of breast tissues for visible and near-infrared radiation (NIR) light.

Key words: random walks, optical imaging, spatial resolution

I. INTRODUCTION

There is great enthusiasm in the optics community to use nonionizing visible or near infrared radiation to image biological targets, such as tumors or internal regions of hemorrhage, that are hidden in optically thick turbid tissues.[1,2] In particular, special attention has been devoted to developing a method to screen for breast cancer. Since in these cases conventional transillumination often provides only very poor resolution,[3] several research groups have proposed employing time-resolved[4–6] or frequency-resolved[7–9] techniques. At this stage of research, various experiments[10–12] and numerical simulations[13,14] have been performed to evaluate critical aspects of such techniques, including the spatial resolution, signal to noise ratio, and detectability of hidden objects.

Collimated light transmitted through thick tissues is scattered many times within a distance of 1 mm (Refs. 15 and 16) and becomes so diffuse by depths of more than a centimeter that deep abnormalities with strong absorption are poorly resolved. Time-resolved transillumination imaging seeks to improve resolution by selecting those photons which have shorter path lengths (early arrival times) and hence smaller deviations from the optical axis (straight line path between the source and the detector). The spatial spread of light in a plane parallel to the surface can be used as a criterion of the spatial resolution of an absorbing object at that depth. This dispersion in photon paths from the optical axis depends on the gating time (path length selection) as well as on the optical properties of the medium. For small-area illumination and detection, the spread of the light is maximal at the middle of the slab. Hence, the worst resolution occurs when the hidden target is located at the midplane.

To compute the spread of light at the middle of a slab, we use random walk models which were developed in our previous investigations of diffusion of light in tissue.[17–20] In Sec. II, we start by analyzing a random walk on an equivalent isotropic scattering lattice bounded by two absorbing planes. In previous publications we showed how the lattice parameters can be expressed in terms of "transport corrected" cross sections which suitably account for the angular anisotropy in the scattering process.[19] An expression for the spread at midslab of those photons injected normally into the medium and detected on the optical axis opposite the point of injection is derived. In Sec. III we compare our theoretical findings with previously published experimental data.[21] Results are discussed in Sec. IV.

II. THEORY

We now use photon migration on a discrete lattice to compute the spread function at the midplane of a slab of thickness N. We derive the joint probability, $\Gamma(\rho,\Delta n)$, that a photon will cross the midslab at a radial distance ρ units from the point of insertion, and that it will take a total of $n=N+\Delta n$ steps, given that it emerges at a detector located coaxially with the point of insertion (see Fig. 1). The quantity $\Delta n=n-N$ represents the number of steps by which the path exceeds the minimum needed to traverse a slab of a given thickness. The basic methodology of the random walk theory that we employ is described elsewhere.[17,20]

First, we define a conditional probability, $U_{l,n}(\rho)$, of those photons which have crossed the midplane of the slab at the point $(x,y,N/2)$ after l steps and have been transmitted through the slab in n steps in total. Since we are interested in those photons which arrive at the point $(0,0,N)$, this conditional probability can be written as

$$U_{l,n}=\frac{1}{6}Q_l\left[x,y,\frac{N}{2}\,|\,0,0,1\right]Q_{n-1-l}\left[0,0,N-1\,|\,x,y,\frac{N}{2}\right], \quad (1)$$

where the first term of the product is the probability of a photon being at $(x,y,N/2)$ after l steps having started at $(0,0,1)$ on the first step, and the second term is the probability of photons being transmitted through the slab to the

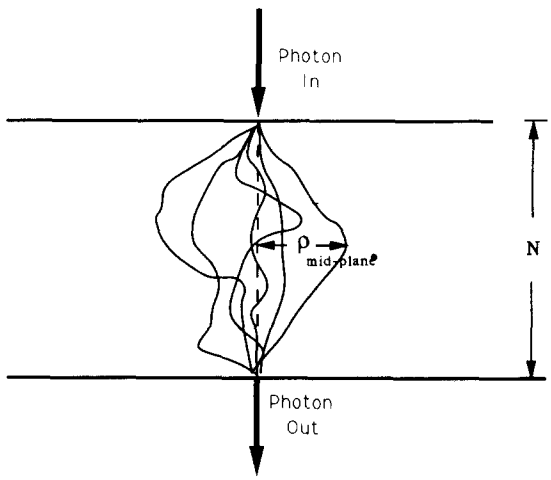

FIG. 1. Schematic representation of photon paths in a transillumination experiment. The spread of light is maximal at the midslab position.

point $(0,0,N-1)$ in $n-1-l$ steps having initially been at the midplane [i.e., $(x,y,N/2)$]. We are interested in the radial dispersion of photons when they are at the midplane (depth $z=N/2$). This quantity can be determined from the probability density obtained by integrating $U_{l,n}(\rho)$ over l

$$W_n(\rho)=\int_0^n U_{l,n}(\rho)dl. \tag{2}$$

Because we are considering an optically homogeneous medium, Q_l can be written in general form as follows:[20]

$$Q_l[\rho,z|0,z_0]=\sum_{k=-\infty}^{\infty}[P_l(\rho,z-z_0+2kN) -P_l(\rho,z+z_0+2kN)], \tag{3}$$

where $P_l(\rho,z)$ is an infinite space propagator that is an even function of ρ and z. Hence, $U_{l,n}$ can be written as

$$U_{l,n}=\frac{1}{6}\sum_{k=-\infty}^{\infty}\left[P_l\left(\rho,\frac{N}{2}-1+2kN\right)-P_l\left(\rho,\frac{N}{2}+1+2kN\right)\right]\sum_{m=-\infty}^{\infty}\left[P_{n-1-l}\left(\rho,\frac{N}{2}-1+2mN\right) -P_{n-1-l}\left(\rho,\frac{3N}{2}-1+2mN\right)\right]. \tag{4}$$

But, because the summations extend from $(-\infty)$ to $(+\infty)$, and because $P_l(\rho,z)$ is an even function of z, it is a straightforward matter to show that the last sum in the above equation can be expressed as $\Sigma_{m=-\infty}^{\infty}P_{n-1-l}(\rho,3N/2-1+2mN)=\Sigma_{m=-\infty}^{\infty}P_{n-1-l}(\rho,N/2+1+2mN)$. Hence, $W_n(\rho)$ may be written as

$$W_n(\rho)=\frac{1}{6}\int_0^{n-1}Q_l\left[x,y,\frac{N}{2}\,|0,0,1\right]\times Q_{n-1-l}\left[x,y,\frac{N}{2}\,|0,0,1\right]dl, \tag{5}$$

which has the form of a convolution integral. $W_n(\rho)$ thus can be calculated according to

$$W_n(\rho)=\tfrac{1}{6}\mathcal{L}^{-1}([\hat{Q}_s(\rho,z|0,1)]^2), \tag{6}$$

where $\hat{Q}_s$ is the Laplace transform of the probability Q_l, and $\mathcal{L}^{-1}$ denotes the inverse transform evaluated at the time point $n-1$.

We use, for the infinite space propagator, the expression

$$P_l(\rho,z)=\left(\frac{3}{2\pi\Delta l}\right)^{3/2}\exp\left(-\frac{3[\rho^2+z^2]}{2\Delta l}\right). \tag{7}$$

The choice of Eq. (7) is based on the following considerations. Let us examine the value $l=N'$, where N' is the minimum time (minimum number of steps) necessary for a photon to reach a plane located at $z=z'$. Clearly, if $\Delta l=l-N'$ is zero, then $Q_l(\rho,z|0,z_0)=\delta(\rho)\delta(z-z')$ in accord with Eqs. (3) and (7). The reason for using the index Δl in Eq. (7) is that we are interested only in the dispersion of the photons relative to those photons which travel directly to the plane in minimal time. The central limit theorem then allows us to approximate this function by a Gaussian form. In Eq. (5) the variable $n-1$ similarly should be taken to be Δn. We thus find that $\hat{Q}_s$ may be expressed as[22]

$$\hat{Q}_s=\mathcal{L}\left[\sum_{k=-\infty}^{\infty}\left(\frac{3}{2\pi\Delta l}\right)^{3/2}\left[\exp\left(-\frac{\alpha_1(k)}{\Delta l}\right)-\exp\left(-\frac{\alpha_2(k)}{\Delta l}\right)\right]\right] =\left(\frac{3}{2\pi}\right)^{3/2}\sum_{k=-\infty}^{\infty}\left[\left(\frac{\pi}{\alpha_1(k)}\right)^{1/2}e^{-2[\alpha_1(k)s]^{1/2}} -\left(\frac{\pi}{\alpha_2(k)}\right)^{1/2}e^{-2[\alpha_2(k)s]^{1/2}}\right], \tag{8}$$

where

$$\alpha_1(k)=\frac{3}{2}\left[\rho^2+\left[\frac{N}{2}-1+2kN\right]^2\right], \tag{9}$$

and

$$\alpha_2(k)=\frac{3}{2}\left[\rho^2+\left[\frac{N}{2}+1+2kN\right]^2\right]. \tag{10}$$

Finally, we note that $W_{\Delta n}(\rho)$ can be viewed as the joint probability $\Gamma(\rho,\Delta n)$ as previously defined. Hence, after taking the inverse Laplace transform required by Eq. (6), we find the following expression for $\Gamma(\rho,\Delta n)$:

$$\Gamma(\rho,\Delta n)=\frac{9}{16\pi^{5/2}(\Delta n)^{3/2}}\sum_{k=-\infty}^{\infty}\sum_{m=-\infty}^{\infty}\left[\frac{\alpha_1(k)^{1/2}+\alpha_1(m)^{1/2}}{\alpha_1(k)^{1/2}\alpha_1(m)^{1/2}}e^{-[\alpha_1(k)^{1/2}+\alpha_1(m)^{1/2}]^2/\Delta n}\right.$$
$$\left.-2\frac{\alpha_1(k)^{1/2}+\alpha_2(m)^{1/2}}{\alpha_1(k)^{1/2}\alpha_2(m)^{1/2}}e^{-[\alpha_1(k)^{1/2}+\alpha_2(m)^{1/2}]^2/\Delta n}+\frac{\alpha_2(k)^{1/2}+\alpha_2(m)^{1/2}}{\alpha_2(k)^{1/2}\alpha_2(m)^{1/2}}e^{-[\alpha_2(k)^{1/2}+\alpha_2(m)^{1/2}]^2/\Delta n}\right]. \quad (11)$$

In order to express Eq. (11) in real time and space as a function of the effective (isotropic-equivalent) scattering cross section, Σ_s^*, the following substitutions have to be made:[19]

$$N=\frac{\Sigma_s^* d}{\sqrt{2}},\quad \Delta n=\Sigma_s^* c\Delta t,\quad \rho=\frac{\Sigma_s^* r}{\sqrt{2}}, \quad (12)$$

where d and r are, respectively, the actual thickness and distance and c is the speed of light in tissue. The quantity Δt is the excess time by which a photon is delayed in reaching the detector when compared with the time of flight through the slab without any scattering. With the substitutions given in Eq. (12), the expression given in Eq. (11) can be viewed as the point spread function of light (PSF) in the midslab for an excess time of flight equal to Δt. Thus, with a constant difference in amplitude, Eq. (11) is also the line spread function (LSF) in the midslab. The latter is the spread of a point source due to the scattering properties of a medium, when viewed in two dimensions.

III. RESULTS

A. Theoretical results

There are several ways to characterize the spatial resolution of an imaging system. One common way is by measuring the width of the LSF, for which the full width at half maximum (FWHM) is 2.35σ if the LSF is Gaussian distributed with a standard deviation, σ. Whereas the expression given in Eq. (11) has a very complicated form, our computation indeed shows that it is well fitted by a Gaussian distribution, particularly for Δn less than the mean transit time. Figure 2 shows the line spread functions in the midplane of thickness $N=7.2$ for several values Δn where the lines are least square fits of a Gaussian to these results.

We followed the same methodology to compute the standard deviation of the fitted Gaussian to determine the LSF for different thickness ($N=7.2$, 11, 21, 31, 41). In Fig. 3, the resulting standard deviations, $\{\sigma\}$, are shown as a function of Δn for various thickness. The interesting result is that the dimensionless spatial resolution is independent of the optical thickness N and only depends on the excess number of steps Δn. Furthermore, data points can be fitted by a power law. The resulting fit gives

$$\sigma=0.406(\Delta n)^{1/2}, \quad (13)$$

where σ is expressed in units of mean effective scattering length, Σ_s^{*-1}. By using the substitutions given in Eq. (12), the standard deviation of the LSF becomes, in terms of real distance

$$\Delta x_\sigma=0.406\left(\frac{c\Delta t}{\Sigma_s^*}\right)^{1/2}. \quad (14)$$

Alternatively, if one were to use the full width at half maximum (FWHM) or full width at tenth maximum (FWTM) as a measure of the resolution, the multiplicative constant in the above expression would be, respectively, 0.94 or 1.17.

It is seen from Eq. (14) that any desired resolution is achievable by choosing the excess transit time, Δt, to have a sufficiently small value. Furthermore, the theoretical spatial resolution is independent of the actual thickness of the slab, but for a given Δt the resolution is inversely proportional to the square root of scattering cross section. The latter inference may seem counterintuitive until one realizes that photons which scatter in a medium with small Σ_s^* (i.e., large mean effective free path) typically will de-

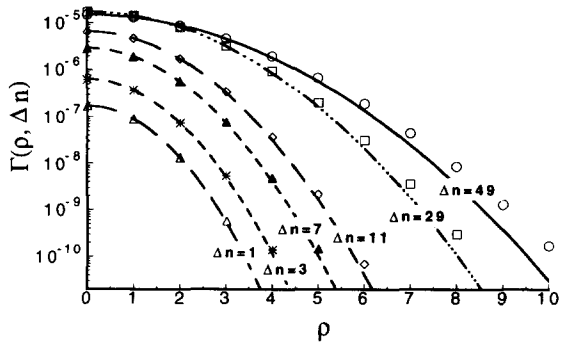

FIG. 2. The line spread $\Gamma(\rho,\Delta n)$, calculated according to random walk theory by Eq. (11). The lines through the data points are Gaussian fits used to obtain values for σ. The value of the thickness here is taken to be $N=7.2$.

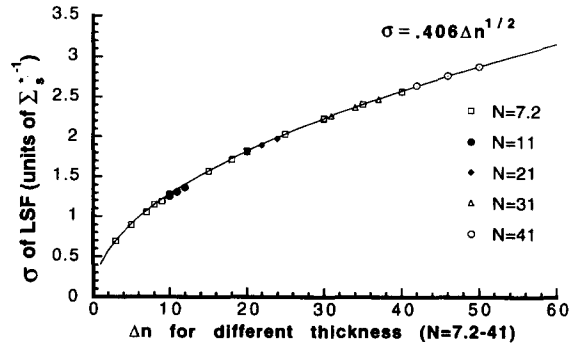

FIG. 3. The standard deviation, σ, as a function of excess numbers of steps, Δn. The solid line is a power law fit to the data points, $\sigma\sim(\Delta n)^{1/2}$.

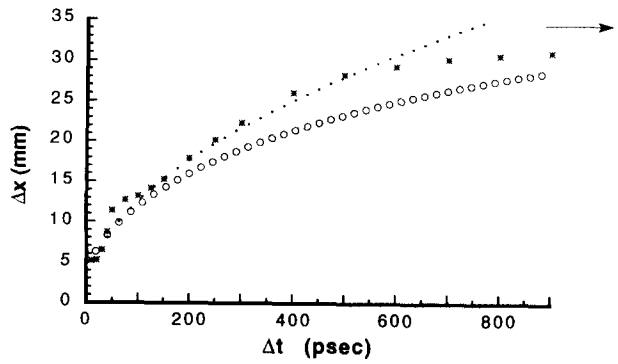

FIG. 4. Comparison between our theoretical calculations of spatial resolution and Hebden's experimental results (Ref. 21). Key: (···) spatial resolution for photons collected at a time Δt in excess of the minimal transit time, calculated according to Eq. (15); (○) spatial resolution calculated from the *mean* excess transit time $\langle \Delta t \rangle$, obtained by using Eqs. (16) and (15); (*) Hebden's data.

viate more from the optical axis than those moving in a highly scattering medium, given that the total path length from the source to the detector is the same. Note that although the resolution improves as Δt decreases, the amount of transmitted detected light decreases very rapidly (see next section).

B. Comparison with experimental results

We now compare our theoretical results with experimental data obtained by Hebden.[21] In Hebden's experiments, a streak camera was used to record the edge response function (ERF) obtained by imaging the abrupt edge of an opaque embedded mask, the photons arriving at times up to a given Δt were summed, and the resulting ERF was fit to a functional form by assuming a Gaussian LSF following Bentzen.[23] Instead of using the FWHM of the LSF, which is equal to 2.35σ, Hebden fit his data to the FWTM of the apparent LSF for which the resolving power of the imaging system can be expressed as

$$\Delta x = \frac{2\pi\sigma(\Sigma_s^*)^{-1}}{\sqrt{(2\ln 10)}} = 1.17\left(\frac{c\Delta t}{\Sigma_s^*}\right)^{1/2}. \tag{15}$$

These experiments were performed with a blackened 150 mm × 100 mm × 51 mm container filled with an aqueous suspension of latex microspheres. By knowing the microsphere diameter (1.27 μm), the concentration (0.07%), and the refractive index (1.59), it is possible to calculate from Mie theory the mean cosine of the scattering angle ($g=0.93$) and the "transport corrected" scattering cross section [$\Sigma_s^* = \Sigma_s(1-g) = 0.2\ \text{mm}^{-1}$]. According to Eq. (11), one can thus compute the LSF and the associated σ for different values of the gating times. In Fig. 4, we compare the spatial resolution calculated according to Eq. (15), illustrated by the dotted line, with the experimental resolution (Δx) obtained by Hebden.[21] No adjustable parameters are used in this comparison.

Although results computed from Eq. (15) fit the experimental data very well for short gating times, the asymptotic limit pertaining to experimental dc measurement is not well represented. This can be explained by the fact that the expression given in Eq. (15) pertains to the resolution at the excess transit time Δt, whereas Hebden's experiments were performed by integrating the signal *up to* Δt. In the latter case the detected signal is the summation of all individual intensities for different time windows, so each time window is weighted by the corresponding intensity. This is the reason why, for delay times greater or equal to the mean transit time of photons, the experimentally observed spread of the integrated edge response function tends to an asymptotic value, viz., that of dc resolution. Hence, to predict the resolution measured in such experiments, we calculated the mean excess transit time $\langle \Delta t \rangle$ for each time window, and substituted it for the discrete time Δt in Eq. (15).

For any distribution $\Gamma'(n)$ of path lengths of photons transmitted through the slab and detected at the optical axis, the mean number of excess steps for a given maximal value $\tilde{n}$ can be calculated as

$$\langle \Delta n \rangle = \frac{\int_0^{\tilde{n}} n\Gamma'(n)dn}{\int_0^{\tilde{n}} \Gamma'(n)dn} - N. \tag{16}$$

We have found in a previous publication[20] that $\Gamma'(n)$ is given by

$$\Gamma'(n) = \frac{\sqrt{3}}{2}\left[\frac{1}{2\pi(n-2)}\right]^{3/2} \times \sum_{k=-\infty}^{\infty} \{e^{-(3/2)\{[(2k+1)L-2]^2/(n-2)\}} - e^{-(3/2)\{[(2k+1)L]^2/(n-2)\}}\} e^{-\mu n}, \tag{17}$$

where μ is the absorption per effective scattering length (Σ_a/Σ_s^*). [Note the integral of $\Gamma'(n)$ represents the transmittance to a detector of unit area located opposite the point of incidence.] Using Eqs. (17) and (16), we performed numerical computations of $\langle \Delta n \rangle$ for the conditions of Hebden's experiments. By the substitutions given in Eq. (12), we then calculated the corresponding mean values of excess transit time, $\langle \Delta t \rangle$, and used the latter to compute the spatial resolution according to Eq. (15). Open circles shown in Fig. 4 are the results of these computations. We note that when integrating over only short excess transit times the value of $\langle \Delta t \rangle$ is very close to the maximal value of Δt in the time window, whereas for long integration times the mean value tends to the asymptotic value obtained for dc illumination (indicated by the arrow in Fig. 4). The points marked by (*) are Hebden's data. The overall agreement seen in Fig. 4 demonstrates that our theoretical methodology is a useful way to examine the spatial resolution for time-resolved imaging. Aside from the inherent approximations in our theory, the small discrepancies between theory and experiment may be due to uncertainties in the reported optical parameters of the phantom, or noise in the edge response functions. As pointed out in Ref. 21, some discrepancy also is likely due to the finite boundaries of the experimental media, particularly for larger values of the gating time.

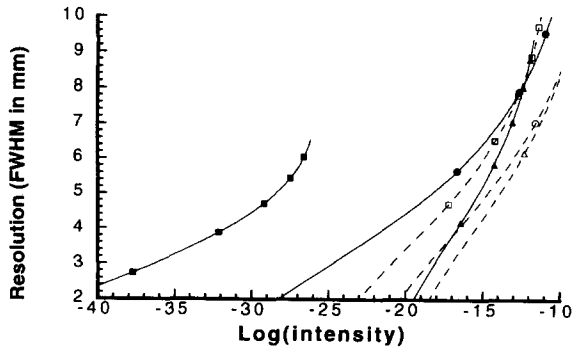

FIG. 5. Expected resolution at the midplane of a 51-mm-thick transilluminated breast as a function of detected intensity, determined for both uniformly adipose (dashed lines) and uniformly grandular (solid lines) tissue, for three different wavelengths (■: 610 nm; ●: 800 nm; ▲: 1250 nm). For these wavelengths, the values in mm^{-1} of the optical coefficients were for adipose tissue: Σ_a (0.05, 0.01, 0.02); Σ_s^*(0.9, 0.8, 0.7) and for glandular tissue: Σ_a (0.2, 0.02, 0.08); Σ_s^* (1.8, 1.2, 0.7).

The latter methodology also can be used to compute the spatial resolution when the medium is absorbing. By using the mean excess transit time, $\langle \Delta t \rangle$, in our calculation, we succeed in obtaining an appropriate weighting, over the gated time windows, of the line spread functions at midplane. Using the calculated mean transit time and Eq. (14), it also becomes rather simple to estimate resolution as a function of detected intensity for time-resolved imaging [cf. Eq. (17)] as the transit time is decreased. The ability to compare detected intensity with resolution for a variety of tissue models becomes critical since we have shown theoretically that any resolutions can be achieved by choosing a small enough Δt. As shown below, the amount of light collected decreases much more rapidly than the width of the LSF.

C. Inferences regarding breast imaging

We now assess possible limitations on breast imaging predicted by our theory. Reported optical parameters for normal adipose (fat) and normal human breast glandular tissues are used in our equations to compare resolution and detected intensity at three wavelengths for a 51-mm thick (compressed between parallel plates as for mammography) breast.

In a recent study Peters *et al.*[24] reported the optical parameters (scattering and absorption coefficients) of excised adipose and glandular breast tissue over a range of wavelengths from visible to infrared light. Using these values, we have computed the expected resolution as a function of detected intensity for homogeneous adipose and homogeneous glandular tissue at three different wavelengths ($\lambda = 610$, 800, 1250 nm). Results are presented in Fig. 5. Because adipose breast tissue has an approximately constant effective mean free path $(\Sigma_s^*)^{-1}$ of about 2 mm for λ within the range 600 to 1250 nm,[24] for the same integration time nearly equivalent resolution is obtained, almost independently of wavelength. However, the intensities are dependent on the absorption of light by hemoglobin (where $a_{610\ nm} > a_{800\ nm} > a_{1250\ nm}$) and are dramatically reduced (3–5 orders of magnitude) at 610 nm for normal tissue blood concentrations. If one requires a time-resolved imaging system to operate at a given intensity (e.g., at a detection limit of 10^{-16}), the imaging resolution for adipose tissue, especially for short excess transit times, would necessarily be worse when the tissue absorption is higher (e.g., 5.3 mm at 610 nm versus 3.6 mm at 1250 nm, as seen in Fig. 5).

In contrast, glandular breast tissue exhibits a strong wavelength dependence of the scattering cross section for values of λ between 610 and 1250 nm.[24] Consequently, as seen in Fig. 5, the resolution curves for the various wavelengths are quite dissimilar. The extremely large loss in the detected intensity with decreasing wavelength, which is particularly evident at higher resolutions (e.g., for FWHM = 3 mm: $\sim 10^{-36}$ at 610 nm; $\sim 10^{-25}$ at 800 nm; $\sim 10^{-18}$ at 1250 nm), can be ascribed mainly to the increase in scattering at short wavelengths.

Thus, the resolution of a totally absorbing object embedded in the middle of an optically homogeneous slab can be significantly improved relative to dc measurements by choosing shorter photon transit times [see Fig. (4)], but at the cost of a dramatically lower detected light level. Similarly, although an increase in scattering cross section will theoretically increase the resolution obtainable for any *given* time gate, the associated decrease in the detected light level will be dramatic, especially at short delay times. If we wish to detect a local abnormality by its optical properties, the contrast of the object relative to its background must be sufficiently large. The largest contrast for an abnormality will occur at wavelengths where either its absorption coefficient is much larger than, or where its scattering cross section is very different from, that of the surrounding tissue. Yet if we choose wavelengths in the near infrared where the tissue absorption is not strong, it is unlikely that a small abnormality will have a high enough absorption relative to the background to give much contrast.

Clearly, as one changes the position of the probe beam, intensities and resolutions can differ widely if the optical parameters of the bulk media vary (e.g., due to varying amounts of adipose and glandular tissue). Hence, deep tissue imaging will be sensitive to the fact that most tissues are not optically homogeneous even over short photon paths. Although breast tissue of young, nonobese women may be overwhelmingly glandular, there is a general trend with age (as well as multigravidas, post menopause, or obesity) for the replacement of glandular with adipose tissue. Thus, x-ray contrast mammography of women over 40 shows tremendous large scale (on the order of cm) spatial variations resulting from adipose replacement of glandular tissue,[25] which complicates the task of detecting abnormal inclusions. Such heterogeneity is likely to cause even greater complication in optical mammography, given the latter's inherently poorer resolution.

In Fig. 6, we compare the ratio, for adipose versus glandular breast tissues, of the predicted optical intensities transmitted through 51 mm tissue. For red/near infrared

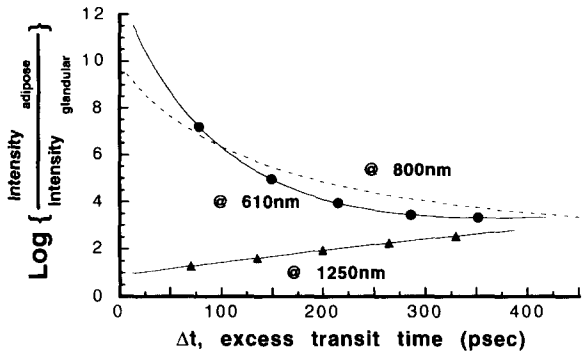

FIG. 6. Log of the ratio of the intensity detected through 51 mm of adipose breast tissue to that of 51 mm of glandular breast tissue as a function of excess transit time (Δt) for three wavelengths. For two wavelengths (610 nm: ●; 800 nm: dashed line); the scattering lengths are significantly less for glandular tissue than for adipose, whereas at 1250 nm (▲) the scattering is the same in adipose and glandular tissue.

wavelengths (610–800 nm), the significantly smaller scattering cross sections for adipose tissue lead to dramatically higher transmitted light at early times. Thus, the aforementioned intrinsic spatial heterogeneity of normal breasts of women over 40 (Ref. 25) is likely to create tremendous spatial variations in transmitted light, especially when the time gate is shortened to optimize optical resolution. These intensity variations are much greater than could be expected from optical changes (due, e.g., to blood content) in small volumes (diameter <6 mm) of abnormal tissue, and would appear to preclude reliable early detection of tumors. Interestingly, at these red/near infrared wavelengths, the ratio of transmitted light intensity of adipose to glandular tissue decreases as the integration time approaches that of dc measurements. The extreme difference in early-time intensities, shown in the top two curves of Fig. 6, is principally due to the significant differences in scattering cross sections between adipose and glandular tissue at those wavelengths. This demonstrates that scattering differences in tissues will have even greater effects on time-resolved images than on dc transillumination.

However, at $\lambda \approx 1250$ nm the effective scattering cross sections of normal adipose and glandular tissue are approximately the same.[24] In this case the logarithm of the transmitted intensity ratios depends only on the product of the absorption difference and the transit time (i.e., path length). Thus the background spatial variations of transmitted intensity due to normal compositional variations are smaller at shorter delay times. In such cases (where the tissue essentially is homogeneously scattering), time-resolved imaging may permit detection of abnormalities if their contrast (attenuation relative to background) is sufficiently greater than the spatial variations in absorption attenuation for the normal breast over that path length. At 1250 nm there is little likelihood of strong absorption differences between abnormal and normal tissues. Therefore, such imaging will be possible only if the abnormality exhibits either dramatically higher (if fibrotic or calcified) or lower (if a cyst) scattering than does normal tissue.

Finally, we note that for the case studied here, of a small source and detector, the width of the LSF decreases dramatically as one nears the surfaces. Thus small features with high contrast near either surface (e.g., superficial veins or tumors) are much more likely to be sensed than deeper ones. When spectroscopic imaging is desired, increasing contrast due to absorption may be more critical than increasing resolution through time gating. In such cases, dc measurements at wavelengths where the absorption is high (e.g., at 600 nm due to blood) may provide the best balance between contrast, intensity, and resolution.

IV. SUMMARY AND DISCUSSION

This work provides an analysis of the LSF of a photon pulse as it passes through the midplane of a slab of thick optically turbid media. The standard deviation of a Gaussian fit to the expression obtained for the LSF is used as a criterion to define the spatial resolution of a time-resolved imaging system. Our results suggest that the spatial resolution is proportional to the square root of the excess transit time, Δt, of the imaging system and inversely proportional to the square root of the scattering cross section, Σ_s, of the medium, as presented in Eq. (14). The theoretical findings have been compared with actual experimental data,[21] with which they are in quite good agreement.

Our theoretical expressions for optical resolution and detected intensity can be used to estimate performance of any time-gated or dc optical imaging of turbid media for which the bulk scattering and absorption parameters are known. We have shown that, in optically homogeneous tissues, time-gating experiments can improve the spatial resolution achieved with an imaging system. Although there is a tremendous loss in the detected intensity for short gating times and thick tissues, one might overcome this difficulty by averaging measurements over many pulses for long enough periods.

For a given tissue thickness, the intensity of a time-gated image is greatly increased as the optical thickness N [expressed in terms of $(\Sigma_s^*)^{-1}$] is reduced. Hence, time-gated imaging of thick tissues such as the human breast is more practical for longer wavelengths (i.e., near infrared), for which smaller values of Σ_s^* result in lower optical thicknesses. dc transillumination exhibits the poorest resolution when absorption is low, in which case the ratio of the excess path to the direct path, $\langle \Delta n \rangle / N$, is relatively large. Therefore, in cases of low tissue absorption (i.e., when using near infrared light), time-gated imaging will improve image resolution relative to dc transillumination. However, due to weak intrinsic biological absorption, one's ability to discern the low contrast due to absorption within a small (e.g., 6 mm) tissue abnormality is problematic when using near-infrared wavelengths; even fivefold increases in the dominant absorbing species (e.g., hemoglobin) will not result in a large change in the detected intensity. Time-resolved imaging that relies on short, less diffuse paths will be less sensitive to absorption changes than dc imaging, but more sensitive to large scattering changes associated with voids/cysts (low scattering) or desmoplastic fibrosis (high scattering).

Over distances of but a few centimeters, human tissues unfortunately exhibit optical heterogeneity deriving from normal compositional variations. These differences (such as the large scattering differences between adipose and glandular breast tissues when λ is in the range of 600 to 800 nm) can lead to variations in detected intensities of many orders of magnitude. Hence, identification of small abnormalities within normal "heterogeneous" tissue becomes very difficult, even when the optical properties of the abnormality differ markedly from those of the surrounding tissue. For breast screening, we have shown that a time-resolved measurement is most likely to be useful when the scattering cross sections of normal tissues are quite similar. Although the exact relationship between the *ex vivo* thin tissue data given in Ref. 24 and the absorption and scattering values for *in vivo* tissue yet needs to be established, existing *ex vivo* data[24] indicate that adipose and glandular tissues scatter similarly and absorb weakly at 1250 nm. In this case small tissue abnormalities also are unlikely to absorb strongly, so any significant image contrast would have to arise from scattering differences between the abnormal and normal tissues.

[a]Physical Sciences Laboratory, Division of Computer Research and Technology.
[b]Biomedical Instrumentation and Engineering Program, National Center for Research Resources.

[1]SPIE Proceedings on Time Resolved Spectroscopic Imaging in Tissues **1431**, (1991).
[2]SPIE Proceedings on Photon Migration and Imaging in Random Media and Tissues **1888** (1993).
[3]B. Monsees, J. M. Destouet, and D. Gersell, "Light scan evaluation of nonpalpable breast lesions," Radiology **163**, 467–470 (1987).
[4]D. T. Delpy, M. Cope, P. Van der Zee, S. Arridge, and J. Wyatt, "Estimation of optical path length through tissue from direct time of flight measurement," Phys. Med. Biol. **33**, 1433–1442 (1988).
[5]J. C. Hebden and R. A. Kruger, "Transillumination imaging performance: A time of flight imaging system," Med. Phys. **17**, 351–356 (1991).
[6]K. M. Yoo, Q. Xing, and R. R. Alfano, "Imaging objects hidden in highly scattering media using femtosecond second-harmonic generation cross-correlation time gating," Opt. Lett. **16**, 1019–1021 (1991).
[7]J. R. Lakowicz and K. Berndt, "Frequency-domain measurements of photon migration in tissue," Chem. Phys. Lett. **166**, 246–252 (1990).
[8]A. Knuttel, J. M. Schmitt, and J. R. Knutson, "Spatial localization of absorbing bodies by interfering diffusive photon-density waves," Appl. Opt. **32**, 381–389 (1993).
[9]J. Fishkin and E. Gratton, "Propagation of photon density waves in strongly scattering media containing an absorbing semi-infinite plane bounded by a straight edge," J. Opt. Soc. Am. A **10**, 127–140 (1993).
[10]S. Andersson-Engels, R. Berg, S. Svanberg, and O. Jarlman, "Time-resolved transillumination for medical diagnostics," Opt. Lett. **15**, 1179–1181 (1990).
[11]M. D. Duncan, R. Mahon, L. L. Tankersley, and J. Reintjes, "Time-gated imaging through scattering media using stimulated Raman amplification," Opt. Lett. **16**, 1868–1870 (1991).
[12]D. A. Benaron and D. K. Stevenson, "Optical time-of-flight and absorbance imaging of biologic media," Science **259**, 1463–1466 (1993).
[13]H. Key, E. R. Davies, P. C. Jackson, and P. N. T. Wells, "Monte Carlo modeling of light propagation in breast tissue," Phys. Med. Biol. **36**, 591–602 (1991).
[14]S. Havlin, J. E. Kiefer, B. Trus, G. H. Weiss, and R. Nossal, "Numerical method for studying the detectability of inclusions hidden in optically turbid tissue," App. Opt. **32**, 617-627 (1993).
[15]S. T. Flock, B. C. Wilson, and M. S. Patterson, "Total attenuation coefficients and scattering phase functions of tissues and phantom materials at 633 nm," Med. Phys. **14**, 835–841 (1987).
[16]S. L. Jacques, C. A. Alter, and S. A. Prahl, "Angular dependence of HeNe laser light scattering by human dermis," Lasers Life Sci. **1**, 309–333 (1987).
[17]R. Bonner, R. Nossal, S. Havlin, and G. H. Weiss, "Model of photon migration in turbid biological media," J. Opt. Soc. Am. A **4**, 423–432 (1987).
[18]R. Nossal, R. F. Bonner, and G. H. Weiss, "Influence of path length on remote optical sensing of properties of biological tissue," Appl. Opt. **28**, 2238–2244 (1989).
[19]A. H. Gandjbakhche, R. Nossal, and R. F. Bonner, "Scaling relationships for theories of anisotropic random walks applied to tissue optics," Appl. Opt. **32**, 504–516 (1993).
[20]A. H. Gandjbakhche, G. H. Weiss, R. F. Bonner, and R. Nossal, "Photon path length distributions for transmission through optically turbid slabs," Phys. Rev. E **48**, 810–818 (1993).
[21]J. C. Hebden, "Evaluating the spatial resolution performance of a time-resolved optical imaging system," Med. Phys. **19**, 1081–1087 (1992).
[22]G. E. Roberts and H. Kaufman, *Table of Laplace Transforms* (Saunders, Philadelphia, PA, 1966).
[23]S. M. Bentzen, "Evaluation of the spatial resolution of a CT scanner by direct analysis of the edge response function," Med. Phys. **10**, 579–581 (1983).
[24]V. G. Peters, D. R. Wyman, M. S. Patterson, and G. L. Frank, "Optical properties of normal and diseased human breast tissues in the visible and near infrared," Phys. Med. Biol. **35**, 1317–1334 (1990).
[25]E. S. deParedes, *Atlas of Film-Screen Mammography* (Urban and Schwarzenberg, Baltimore, MD, 1992).